

RS Flip-Flop Circuit Dynamics Revisited

Aminur Rahman

Department of Mathematical Sciences
New Jersey Institute of Technology
Newark, NJ 07102-1982
ar276@njit.edu

* *

Denis Blackmore

Department of Mathematical Sciences
New Jersey Institute of Technology
Newark, NJ 07102-1982
denis.l.blackmore@njit.edu

Abstract

Logical RS flip-flop circuits are investigated once again in the context of discrete planar dynamical systems, but this time starting with simple bilinear (minimal) component models based on fundamental principles. The dynamics of the minimal model is described in detail, and shown to exhibit some of the expected properties, but not the chaotic regimes typically found in simulations of physical realizations of chaotic RS flip-flop circuits. Any physical realization of a chaotic logical circuit must necessarily involve small perturbations - usually with quite large or even nonexistent derivatives - and possibly some symmetry-breaking. Therefore, perturbed forms of the minimal model are also analyzed in considerable detail. It is proved that perturbed minimal models can exhibit chaotic regimes, sometimes associated with chaotic strange attractors, as well as some of the bifurcation features present in several more elaborate and less fundamentally grounded dynamical models that have been investigated in the recent literature. Validation of the approach developed is provided by some comparisons with (mainly simulated) dynamical results obtained from more traditional investigations.

Keywords: RS flip-flop circuits, minimal model, Neimark–Sacker bifurcation, chaos, chaotic strange attractors, Smale horseshoe

AMS Subject Classification: 37C05, 37C29, 37D45, 94C05

Since the advent of electronic computing devices, flip-flops have played a major role in processing arithmetic operations. The first flip-flop to be designed was the RS flip-flop (RSFF). It has the ability to store bits, and hence was used in adders and primitive electronic calculators. The RSFF was even used in the video game “pong”. The only logical flaw of this circuit is the ambiguity of the output when the inputs are both high voltage. In order to rectify this flaw other flip-flops were designed. In the 1980s Leon Chua designed the simplest circuit to exhibit chaos. In more recent years, Chua’s circuit and the flaw of the RSFF have been exploited to design chaotic flip-flops. These chaotic flip-flops have the potential to be employed in random number generation, encryption, and fault tolerance. However, in order to exploit their properties they need to be studied further. Since experiments with large systems become difficult, tractable mathematical models that are amenable to analysis via the tools of dynamical systems theory are of particular value. The model needs to be simple enough to simulate with ease and agree qualitatively with experiments for small systems. We model the RSFF circuit as a discrete dynamical system - called the minimal model - focusing on the ambiguous output case. The minimal model is perturbed in various ways to reproduce qualitative behavior observed in experiments for the chaotic RSFF, and the minimal approach can be readily generalized to handle other logical circuits.

1 Introduction

Logical circuits are constructed using logic gates representing propositional connectives such as AND (conjunction), OR (disjunction) and their negation. They, or more precisely physical approximations of ideal logical circuits, have important applications in multiplexers, registers, pseudo-random number generators, quantum network modeling and, in fact, virtually every microprocessor (see, e.g.[3]). Consequently, having efficient methods for analyzing and predicting their behavior, such as by continuous or discrete dynamical systems models is of great value in design, analysis and evaluation.

A well-known example with many applications (*e.g.* in quantum networks [34]) is the RS

Flip-Flop circuit in Fig.1, which is a feedback circuit comprising two NOR gates (which are negations of OR gates). Note that an OR gate has an output of 1 when at least one of the inputs is 1 and an output of 0 when both inputs are zero, with 1 denoting true and 0 false. An ideal *RS flip-flop circuit* (*RSFF circuit*) is a logical feedback circuit represented in Fig. 1, with input/output behavior described in Table 1, which shows the *set* (*S*) and *reset* (*R*) inputs for the circuit consisting of two *NOR gates* with outputs *Q* and *Q'*. The input to the output, denoted by $(Q_n, Q'_n) \rightarrow (Q_{n+1}, Q'_{n+1})$ may be regarded as the action of a map from the plane $\mathbb{R}^2 := \{(x, y) : x, y \in \mathbb{R}\}$ into itself, where \mathbb{R} denotes the real numbers and in the ideal case, the coordinates assume the binary values $\{0, 1\}$. This suggests that the behavior of the RSFF circuit might possibly be effectively modeled by the iterates of a planar map, which comprise a discrete dynamical system (DDS), and its perturbations derived directly - albeit in a simplified manner - from a faithful interpretation of the circuit itself. And this is our focus in the sequel, which should be contrasted with our prior investigation [2]. The model to be studied in what follows, fundamentally grounded as it is in the basic principles of ideal logic circuit theory, is substantially more compelling and useful than the one investigated in [2], which was primarily an *ad hoc* construct designed to mimic the known behavior of RSFF realizations.

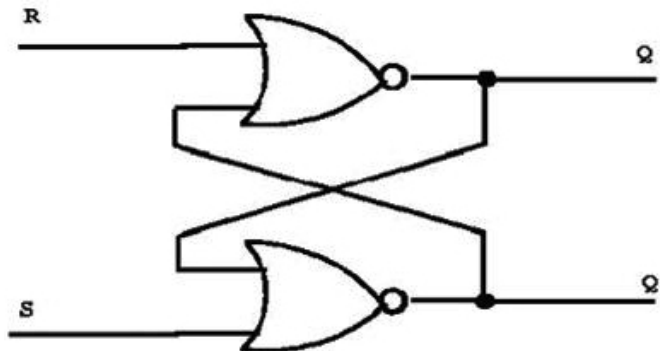


Figure 1: *R-S* flip-flop circuit

The binary input/output behavior, with 0 and 1 representing false and true, respectively, is given in the following table.

<i>S</i>	<i>R</i>	$S_1 := Q$	$R_1 := P$
1	0	1	0
0	1	0	1
1	1	0	0
0	0	1 or 0	0 or 1

Table 1. Binary input/output of R - S flip-flop circuit

From the DDS perspective, our first goal is to construct the simplest map of the plane (based on bilinear representations of the NOR gates) that models the logical properties of the RSFF circuit, with iterates that exhibit most of the interesting properties that follow from basic analysis or have been observed in the dynamics of physical realizations and their mathematical models. This begs the question of how the dynamics of the planar map models are to be compared with that obtained directly from measurements of physical realizations of the RSFF circuit and its flip-flop relatives and the analysis and simulations of the usual mathematical models, which we shall endeavor to address in what follows.

The usual form of the mathematical models is traceable back to the pioneering work of Moser [24] ; namely, associated three-dimensional systems of piecewise-smooth, first-order, nonlinear autonomous ordinary differential equations (ODEs) obtained from applying Kirchhoff's laws to the realizations. These realizations typically comprise such elements as capacitors, inductors and nonlinear resistors and exhibit highly oscillatory, very unstable and even chaotic dynamics (*metastable operation*), as experimentally observed in such studies as [16, 17, 21], where tunnel diodes of the type used in Chua's circuit (see [4, 6, 7, 26]) are the key ingredients in the construction of the nonlinear resistors. There are several connections between the solutions of the model ODEs and iterates of maps that can be used for dynamical comparisons, among which are the following: as observed by Hamill *et al.* [13], the autonomous nature of the logical circuit equations allows dynamical analysis via the iterates (snapshots) of a fixed time map, which can be reduced to a planar map in special cases as shown in Kacprzak and Albicki [16] and Kacprzak [17]. In addition, the application of a standard explicit one-step integration method is tantamount to the iteration of the map describing the scheme, thus enabling the (approximate) reduction from a continuous to a discrete dynamical system as shown *e.g.* in Danca [8]. Of course, there is the well-known method of employing Poincaré sections to analyze three-dimensional continuous dynamical systems using two-dimensional discrete dynamical systems, which has been employed in numerous investigations of logical circuit realizations such as Cafagna and Grassi [4], Murali *et al.* [26], Okazaki *et al.* [27] and Ruzbehani *et al.* [31].

As it turns out, logical circuits can be realized using the famous circuit of Chua and its generalizations [6, 7], which have depended heavily powerful tools such as Poincaré maps, Melnikov functions and normal forms from the modern theory of dynamical systems and bifurcation theory (see [9, 12, 18, 20, 28, 32, 33]) for their analysis. There is also another interesting connection between realization of logical circuits and nonlinear maps that might afford an opportunity for comparisons with the results obtained from our two-dimensional DDS models; namely, the approach in the work of Ditto *et al.* [11], which features the notion of reconfigurable logic gates comprising connected NOR and NAND gates constructed using

1-dimensional DDS and associated thresholds.

Our investigation begins in Section II, where we define a (minimal) planar map model of an ideal RSFF circuit - derived directly from the logical circuit - that plays a foundational role throughout the sequel. Moreover, we derive some basic properties of the minimal map concerning such things as smoothness and the existence and description of an inverse. This is followed in Section III with a more thorough analysis of the fixed points of the minimal map - including a local stability analysis and an analysis of stable and unstable manifolds. As a result of this more detailed investigation, we find that the dynamics is quite regular when the domain of the map is appropriately restricted. Next, in Section IV, after observing that the minimal map is C^1 -structurally stable, we prove that (1-dimensional) chaos can be generated by arbitrarily small C^0 perturbations of the map. In particular, it is shown that a tent map can be embedded in a (1-dimensional) stable manifold of a fixed point by such a perturbation, thereby inducing chaotic tent dynamics. We then prove the existence of several types of more substantial (2-dimensional) chaotic regimes for arbitrarily small C^0 perturbations in Section V. In particular, we show that arbitrarily C^0 small perturbations can be fashioned to produce transverse intersections in homoclinic orbits and heteroclinic cycles that generate chaos, horseshoe chaos, multihorseshoe strange chaotic attractors, and Neimark–Sacker bifurcations. In Section VI, we illustrate our theorems by making liberal use of numerical simulations of our perturbed models. Finally, in Section VII, we briefly summarize our results, describe some interesting areas of application and discuss plans for related future research.

2 A Minimal Discrete Dynamical System Model

To obtain the minimal DDS model for the RSFF circuit, we start with the simplest continuous extension of the input/output map of the NOR gate to the unit square in the plane, which is clearly given by the function $\mathcal{N} : I^2 (\subset \mathbb{R}^2) \rightarrow I (\subset \mathbb{R})$ defined as

$$\mathcal{N}(x, y) := (1 - x)(1 - y), \tag{1}$$

where $I^2 := I \times I := [0, 1] \times [0, 1] \subset \mathbb{R}^2$ is the unit square and x and y are the inputs. Observe that this quadratic function is bilinear in the variables $(1 - x)$ and $(1 - y)$, and behaves precisely like the pure logical NOR gate when $x, y \in \{0, 1\}$. Using the functional representation (1) for each of the (NOR gate) components of the RSFF circuit, we obtain the continuous extension for the RSFF,

$$Q := \frac{S(1 - R)}{R + S - RS}, \quad Q' := \frac{R(1 - S)}{R + S - RS}. \tag{2}$$

Since the threshold outputs are fed back in a similar manner to the RSFF outputs, we make the naive assumption that the logical behavior is preserved and we readily obtain its minimal extension to the unit square in the form of a map $F : I^2 \rightarrow I^2$ defined as

$$F = (\xi, \eta) : I^2 \ (\subset \mathbb{R}^2) \rightarrow I^2 \ (\subset \mathbb{R}^2), \quad (3)$$

where the coordinate functions are

$$\xi(x, y) := \frac{y(1-x)}{x+y-xy}, \quad \eta(x, y) := \frac{x(1-y)}{x+y-xy}, \quad (4)$$

with the x - y -coordinates playing the roles of the previous threshold output, and ξ - η coordinates playing the roles of the current threshold output.

This map generates a discrete (semi-) dynamical system in terms of its forward iterates determined by n -fold compositions of the map with itself, denoted as F^n , where $n \in \mathbb{N}$, the set of natural numbers. We shall employ the usual notation and definitions for this system; for example, the *positive semiorbit* of a point $p \in \mathbb{R}^2$, which we denote as $O_+(p)$, is simply defined as $O_+(p) := \{F^n(p) : n \in \mathbb{Z}, n \geq 0\}$, and all other relevant definitions are standard (*cf.* [12, 18, 28, 33]). The minimal map (3) is real-analytic (C^ω) on I^2 except at the origin, where it is not even well-defined. Consequently, we should really consider F to be defined on $I^2 \setminus \{(0, 0)\}$ and actually on $X := I^2 \setminus \{(0, 0), (1, 1)\}$ if we wish to avoid the origin for all forward iterates of F .

2.1 Basic analytical properties of the minimal model

First we take note of some of the analytical properties of the map (3), which are listed in what follows. The proofs of all these results are straightforward and left to the reader.

(A1) The map $F \in C^\omega(X)$.

(A2) F is \mathbb{Z}_2 -symmetric in the sense that

$$R \circ F = F \circ R$$

for the reflection R in the line $y = x$.

(A3) $F(X) = Y := \{(\xi, \eta) \in \mathbb{R}^2 : 0 \leq \xi, \eta \text{ and } \xi + \eta < 1\} \cup \{(1, 0), (0, 1)\}$.

(A4) $F(\{(x, 0) : 0 < x \leq 1\}) = (0, 1)$, $F(\{(0, y) : 0 < y \leq 1\}) = (1, 0)$, and if $\rho(a) := \{(x, ax) : 0 < x, a\} \cap X$ is the ray through the origin sans the origin in X , then $F(\rho(a)) \subset \{(\xi, (a-1) + a\xi) : 0 < \xi\} \cap Y$. Moreover, as $(x, y) \rightarrow (0, 0)$ along the ray $\rho(a)$, $F(x, y)$ converges to the point of intersection of the line defined by $x + y = 1$ with the ray $\rho(1/a)$. This shows just how singular the formulas (3) are at the origin.

(A5) The derivative (matrix) for F on X is

$$F'(x, y) = (x + y - xy)^{-2} \begin{pmatrix} -y & x(1-x) \\ y(1-x) & -x \end{pmatrix}, \quad (5)$$

with determinant

$$\det F'(x, y) = xy(x + y - xy)^{-3}, \quad (6)$$

which, not surprisingly in view of (A3), shows that the implicit function theorem cannot guarantee the existence of a local smooth inverse along the x - and y -axes.

(A6) In fact, the inverse of F , where it exists, is given as

$$F^{-1}(\xi, \eta) = \left(\frac{1 - \xi - \eta}{1 - \eta}, \frac{1 - \xi - \eta}{1 - \xi} \right), \quad (7)$$

which is clearly in $C^\omega(Y \setminus \{(1, 0), (0, 1)\})$.

3 Dynamics of the Minimal Model

We shall analyze the deeper dynamical aspects of the model map (2)-(3) for various parameter ranges in the sequel, but first we dispose of some of the more elementary properties that follow directly from the definition and (A1)-(A6), leaving the simple proofs once again to the reader.

(D1) If we restrict F to $\hat{X} := \{(x, y) : 0 < x, y \text{ and } x + y < 1\}$, and denote this restriction by \hat{F} , it determines a full dynamical system defined as

$$\{\hat{F}^n : n \in \mathbb{Z}\},$$

which, for example, allows the definition of the full *orbit* of a point $p \in \hat{Y}$ as

$$O(p) := \{\hat{F}^n(p) : n \in \mathbb{Z}\}.$$

(D2) The line $y = x$ is F -invariant, while the x - and y -axes are F^2 -invariant.

(D3) Both of the points $(1, 0)$ and $(0, 1)$ are fixed points of F^2 .

3.1 Analysis of the fixed and periodic points

The properties of the fixed and periodic points of our model map shall be delineated in a series of lemmas, which follow directly from the results in the preceding sections and fundamental dynamical systems theory (as in [12, 18, 28, 33]). Our first result is the following, which has a simple proof that we leave to the reader.

Lemma 1. *The only fixed point of F in X is*

$$p_* = (x_*, y_*) = \left(\frac{3 - \sqrt{5}}{2}, 1 \right) \cong 0.38197(1, 1),$$

which is a saddle point with eigenvalues

$$\lambda_s = - \left(\frac{3 - \sqrt{5}}{2} \right), \quad \lambda_u = - \left(\frac{1 + \sqrt{5}}{2} \right).$$

This fixed point has linear stable and stable manifolds given as

$$W_{lin}^s(p_*) = \{(x, x) : x \in \mathbb{R}\} \text{ and } W^s(p_*) = \{(x, x) : 0 < x < 1\},$$

and the linear unstable manifold

$$W_{lin}^u(p_*) = \{(x, -x + 2x_*) : x \in \mathbb{R}\}.$$

Next, we analyze the unstable manifold of p_* in some detail. For this purpose, it is convenient to introduce a change of variables linked to the symmetry of F expressed in (A2); namely,

$$T(x, y) = (u, v) := \left(\frac{x + y - 2x_*}{\sqrt{2}}, \frac{-x + y}{\sqrt{2}} \right),$$

with inverse

$$T^{-1}(u, v) = (x, y) := \left(x_* + \frac{u - v}{\sqrt{2}}, x_* + \frac{u + v}{\sqrt{2}} \right).$$

Clearly, T is a translation of the origin to the fixed point p_* followed by a counterclockwise rotation of $\pi/4$. The defining map for the dynamics in the new coordinates can be readily computed to be

$$\tilde{F}(u, v) := T \circ F \circ T^{-1}(u, v) = \left(\sqrt{2}/R(u, v) \right) \left(\sqrt{2}(1 + 2x_*^2)u + (1 - x_*^2)(v^2 - u^2), -\sqrt{2}v \right), \quad (8)$$

where

$$R(u, v) := 2x_*(2 - x_*) + 2\sqrt{2}(1 - x_*)u + v^2 - u^2.$$

The properties of the unstable manifold of the fixed point may now be described as in the following result, which can be proved directly from Lemma 3.1 and (7).

Lemma 2. *The unstable manifold of the fixed point p_* , which corresponds to $0 = (0, 0)$ in the new uv -coordinates, has the form*

$$W^u(p_*) = W^u(0) = \{(\varphi(v), v) : |v| < 1/\sqrt{2}\},$$

where φ is a smooth (C^∞) function satisfying the following properties:

(i) $\varphi(0) = \varphi'(0) = 0$ and $\varphi(v) \uparrow \frac{-2+\sqrt{5}}{\sqrt{2}}$ as $v \uparrow 1/\sqrt{2}$.

(ii) φ is an even function

(iii) φ satisfies the functional equation

$$\varphi(v) = \kappa \left\{ (1 - x_*^2) (\varphi(v)^2 - v^2) + \frac{S(\varphi(v), v)}{\sqrt{2}} \varphi \left(\frac{-2v}{S(\varphi(v), v)} \right) \right\}, \quad (9)$$

where $\kappa := 1/[\sqrt{2}(1 + 2x_*^2)]$ and

$$S(\varphi(v), v) := 2x_*(2 - x_*) + 2\sqrt{2}(1 - x_*)\varphi(v) + v^2 - \varphi(v)^2.$$

We note here that (8) can be used to obtain Picard iterate (local) approximations of the unique solution via the recursive formula (cf. [14])

$$\varphi_{n+1}(v) = \kappa \left\{ (1 - x_*^2) (\varphi_n(v)^2 - v^2) + \frac{S(\varphi_n(v), v)}{\sqrt{2}} \varphi_n \left(\frac{-2v}{S(\varphi_n(v), v)} \right) \right\}. \quad (10)$$

A good starting point for these iterates is

$$\varphi_1(v) := \sqrt{2} (\sqrt{5} - 2) v^2,$$

which satisfies the first two properties of Lemma 3.2, and turns out to be a fairly good approximation for the unstable manifold. Using (9), we obtain an even better approximation in the form

$$\varphi_2(u) = \kappa \left\{ (1 - x_*^2) \left(2(\sqrt{5} - 2)v^2 - 1 \right) v^2 + (\sqrt{5} - 2) S(\varphi_1(v), v) \left(\frac{-2v}{S(\varphi_1(v), v)} \right)^2 \right\}, \quad (11)$$

where

$$S(\varphi_1(v), v) = 2 \left\{ x_*(1 - x_*) + v^2 \left[\left(2(1 - x_*)(\sqrt{5} - 2) + 1 \right) - (\sqrt{5} - 2)^2 v^2 \right] \right\}.$$

which is illustrated in Fig. 2. As a matter of fact, it can be proved that these iterates actually converge locally to the smooth solution of (8), but the details, which follow the argument

in [14], although straightforward, are a bit too involved to include here. We remark here that it is not difficult to prove that a global solution of the unstable manifold equation can be obtained as follows:

$$W^u(p_*) = \lim_{n \rightarrow \infty} F^n(\Delta'),$$

where $\Delta' := \{(x, 1 - x) : 0 \leq x \leq 1\}$.

Let us now investigate periodic orbits of the dynamical system (2). It is easy to see from the definition that $\zeta := \{(1, 0), (0, 1)\}$ is a 2-cycle in which each point has (least) period two. As for any other cyclic behavior, we have the following comprehensive result that follows directly from the definition of the dynamical system and properties (A1)-(A6) and (D1)-(D3).

Lemma 3. *The 2-cycle $\zeta := \{(1, 0), (0, 1)\}$ is the only cycle of F ; it is superstable and has basin of attraction*

$$\mathfrak{B}(\zeta) := I^2 \setminus \{(x, x) : x \in \mathbb{R}\}.$$

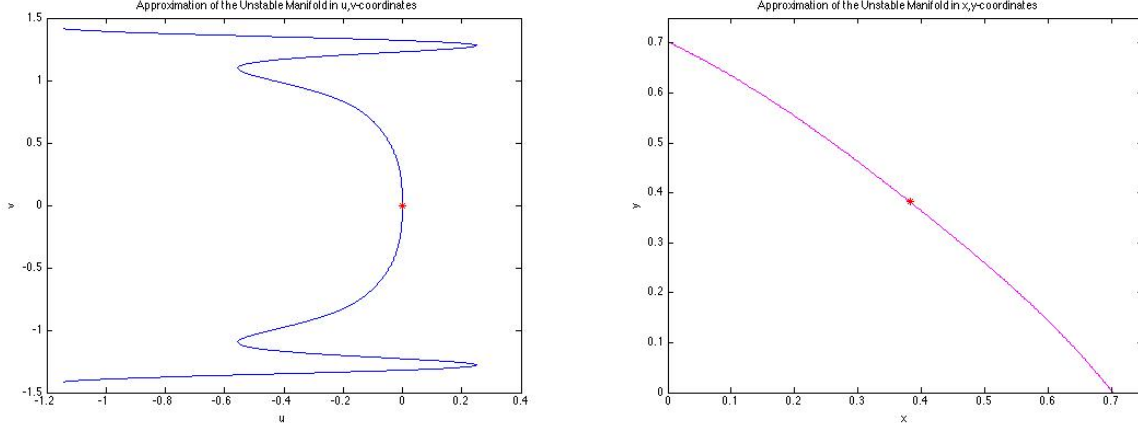


Figure 2: Picard iteration approximation (φ_6) in u, v -coordinates and x, y -coordinates respectively.

3.2 Summary of the dynamics

We see from our analysis that the dynamical system (generated by) F defined by (2)-(3) has highly oscillatory, but quite regular behavior. There is one fixed point (on the line $y = x$), which attracts everything on the diagonal in X . In addition, there are only two other special

points; namely, $(1, 0)$ and $(0, 1)$, both of which are superstable periodic points of period two that comprise the 2-cycle $\zeta := \{(1, 0), (0, 1)\}$. Moreover, ζ attracts everything in X except the points along the diagonal. Thus we see that our minimal model nicely replicates the highly oscillatory “race” behavior found in physical realizations of RSFF circuits, but none of the chaotic dynamics. In fact, the nonwandering set of the minimal dynamical system, which actually coincides with the periodic set, has the very simple form

$$\Omega(F) = \text{Per}(F) = \{p_*\} \cup \zeta, \quad (12)$$

and F is C^1 -structurally stable so that the dynamics maintains its regularity for all perturbations that, along with their derivatives, are sufficiently small. A proof of the structural stability for our map, which does not quite satisfy the usual hypotheses, can be fashioned from a straightforward modification of the methods employed in [9, 28, 29, 30]. Thus, it would seem that perturbations capable of generating chaos can be very small, but their derivatives need to be quite large or even fail to exist. We shall verify this in the sequel.

4 Perturbed Minimal Model with One-dimensional Chaos

In this section we shall show how small perturbations that do not break the reflectional symmetry of the minimal model can produce chaos along the diagonal. More precisely, we shall give a constructive proof of the following result.

Theorem 4. *There exist continuous arbitrarily small C^0 perturbations of the minimal model map F for the RSFF circuit that are symmetric with respect to reflections in the invariant line $y = x$ and exhibit one-dimensional chaos in their restrictions to the diagonal.*

Proof. The idea of our argument is to embed an arbitrarily small C^0 perturbation into F that implants known chaotic dynamics along the dynamics without breaking the symmetry. This chaotic insert is defined along the diagonal for any $\sigma > 0$ using the continuous piecewise-linear function

$$\psi_\sigma(x) := \begin{cases} -x, & -2\sigma \leq x \leq 0 \\ -2(\sigma - |x - \sigma|), & 0 \leq x \leq 2\sigma \end{cases}, \quad (13)$$

which is illustrated in Fig. 8a. Observe that the composition $\tau_\sigma := \psi_\sigma^2 : [0, 2\sigma] \rightarrow [0, 2\sigma]$ is just the 2σ -scaled tent map given by

$$\tau_\sigma(x) = 2(\sigma - |x - \sigma|),$$

which is known to have chaotic dynamics, including periodic orbits of all periods, a dense orbit and a Lyapunov exponent of $\log 2$ for almost all initial points (see, e.g. [18]). Now we

note from the definitions (2) and (3), (A2) and Lemma 3.1 that the restriction f of F to the diagonal is

$$f(x) = \frac{1-x}{2-x}, \quad (14)$$

which has the unique (stable) fixed point $x_* = (1/2)(3 - \sqrt{5})$, and this is a global attractor on the unit interval $[0, 1]$. It is easy to see that for every $\epsilon > 0$, we can choose $0 < 8\sigma < \min\{1/6, \epsilon\}$ such that there is a continuous map $f_\sigma : [0, 1] \rightarrow [0, 1/2]$ with the following properties: (i) $f_\sigma(x) = \psi_\sigma(x - x_*)$ for all $x \in J_\sigma := [x_* - 2\sigma, x_* + 2\sigma]$; (ii) $f_\sigma(x) = f(x)$ for all $x \in [0, 1] \setminus [x_* - 8\sigma, x_* + 4\sigma]$; (iii) f_σ is strictly decreasing on $[0, x_* + \sigma] \cup [x_* + 2\sigma, 1]$; and (iv) $|f_\sigma(x) - f(x)| < 4\sigma$ for all $0 \leq x \leq 1$. We observe that J_σ is a global attractor for f_σ , but not strange since it has dimension equal one. The one-dimensional chaotic implant can be extended to the whole two-dimensional domain of F . More precisely, it is easy to see (by simply linearly joining the perturbed diagonal map to F) that there exists for any $0 < 8\sigma < \min\{1/6, \epsilon\}$ a continuous map $F_\sigma : X \rightarrow X$ satisfying the following properties: (a) the diagonal is F_σ -invariant (b) F_σ restricted to the diagonal is f_σ ; (c) F_σ is symmetric with respect to the diagonal; (d) the dynamics of F_σ of the diagonal are qualitatively the same as that of F ; and (e) $|F_\sigma(x, y) - F(x, y)| < 8\sigma$ for all $(x, y) \in X$. As σ can be made arbitrarily small, the proof is complete. \square

Observe that the perturbation F_σ constructed in the above proof is merely continuous and piecewise smooth inside a small ball centered at the fixed point x_* and smooth (i.e. C^∞) outside of the ball. The perturbation and its chaotic dynamics are illustrated in Fig. 8b. By smoothing the corners of the construction, the perturbation can be made smooth, which leads directly to the following result.

Corollary 5. *The perturbation in Theorem 4 can be chosen so that it is a C^∞ function having the same qualitative dynamics as the function constructed above.*

It is useful to note that the perturbation F_σ producing one-dimensional chaos along the invariant diagonal is arbitrarily C^0 close to the original map F . However, it cannot be made arbitrarily C^1 close to F by virtue of the readily verified fact that the restriction to the diagonal is C^1 -structurally stable, so we cannot find arbitrarily small perturbations in the C^1 sense that possess chaotic dynamics. As we shall see in the next section, there exist arbitrarily small C^1 perturbations of F that are C^∞ and exhibit (two-dimensional) chaotic dynamical regimes.

5 Two-dimensional Chaos Induced by Perturbation

In this section we shall show how arbitrarily small perturbations of the minimal model can induce chaotic dynamics of various types that are more substantial and complex than that described in Theorem 4.1. Our first perturbation involves the (geometric) local embedding of a Smale horseshoe in the minimal model in a neighborhood of the saddle point p_* .

5.1 Direct horseshoe chaos

We begin by defining a map in a neighborhood of p_* that yields the desired horseshoe. First, let $0 < \delta_0 \leq 0.04$ so that

$$\bar{B}_{6\sqrt{2}\delta_0}(p_*) := \{(x, y) \in \mathbb{R}^2 : (x-x_*)^2 + (y-y_*)^2 \leq 72\delta_0^2\} \subset [x_* - 6\sqrt{2}\delta_0, x_* + 6\sqrt{2}\delta_0]^2 \subset (0, 1)^2 = \text{int}(I^2),$$

where $\text{int}(E)$ denotes the interior of the subset E of the plane. Now, for each $0 < \delta \leq \delta_0$, we introduce a (s, t) -coordinate system with origin at p_* , the s -axis pointing to the right along the linear unstable manifold of p_* and the t -axis pointing upward along the stable manifold of p_* . Let $P_\delta : \{(s, t) : |s|, |t| \leq 6\delta\} \rightarrow \mathbb{R}^2$ be defined in terms of s, t -coordinates as

$$P_\delta(s, t) := (\phi_\delta(s), \psi_\delta(s, t)), \quad (15)$$

where ϕ_δ is an odd function such that

$$\phi_\delta(s) := \begin{cases} -(3/2)s, & 0 \leq s \leq 2\delta \\ 3(s - 3\delta), & 2\delta \leq s \leq 4\delta \\ (1/3)(s + 5\delta), & 4\delta \leq s \leq 6\delta \end{cases},$$

and ψ_δ is an odd function of t for each s given by

$$\psi_\delta(s, t) := -\delta t - \mu(s),$$

where

$$\mu(s) := \begin{cases} 0, & |s| \leq 2\delta \\ \text{sgn}(s)(|s| - \delta), & \delta \leq |s| \leq 2\delta \\ \text{sgn}(s)\delta, & |s| \geq 2\delta \end{cases}.$$

As p_* is a fixed point of both P_δ and the minimal model F , for and given $\epsilon > 0$ we can choose $0 < \delta = \delta(\epsilon) \leq \delta_0$ such that in terms of the euclidean norm, we have

$$\|F(p) - P_\delta(p)\| < \epsilon$$

for all $p \in \bar{B}_{6\sqrt{2}\delta_0}(p_*)$. Moreover, it is easy to see - as shown in Fig. 3 - that the image of the square

$$Q_\delta := \{(s, t) : -2\delta \leq s, t \leq 2\delta\}$$

under the map (13), namely $P_\delta(Q_\delta)$, is a (double) horseshoe. Note that all of the above functions are continuous and piecewise linear, which means they have smooth approximations (obtained by smoothly rounding out the corners) that are arbitrarily C^0 -close to them. Consequently, we can and will assume that the perturbations chosen here to prove our next result and in the sequel are smooth.

Theorem 6. *For every $\epsilon > 0$ there exists a $0 < \delta = \delta(\epsilon) \leq 0.04$ such that the (smooth) perturbation of the minimal model map F defined as*

$$F_\delta(p) := (1 - \rho(r)) P_\delta(p) + \rho(r) F(p), \quad (16)$$

where P_δ is as in (15), $r := \|p - p_*\|$ and

$$\rho(r) := \begin{cases} 0, & 0 \leq r \leq 4\delta\sqrt{2} \\ (1/\delta\sqrt{2})(r - 4\delta\sqrt{2}), & 4\delta\sqrt{2} \leq r \leq 5\delta\sqrt{2} \\ 1, & r \geq 5\delta\sqrt{2} \end{cases},$$

satisfies $\|F_\delta(p) - F(p)\| < \epsilon$ for all $p \in I^2$ and $F_\delta(Q_\delta)$ is a double horseshoe as shown in Fig. 3.

Proof. As noted above, the restriction $0 < \delta \leq 0.04$ guarantees that $\bar{B}_{6\sqrt{2}\delta}(p_*)$ is contained in the interior of I^2 and that by taking δ sufficiently small, we can further insure that $\|F(p) - P_\delta(p)\| < \epsilon$ on $\bar{B}_{6\sqrt{2}\delta}(p_*)$. Hence, it follows from the definition of ρ and (16) that $\|F_\delta(p) - F(p)\| < \epsilon$ on I^2 . Finally, (16) implies that $F_\delta(Q_\delta) = P_\delta(Q_\delta)$, which is the double horseshoe illustrated in Fig.3, and this completes the proof. \square

In light of Theorem 6, the next result on the existence of horseshoe type chaos follows directly from the results of Birkhoff, Moser and Smale (*cf.* [12, 18, 25, 28, 30, 32, 33]).

Corollary 7. *The perturbation F_δ in Theorem 6 is chaotic on an invariant subset contained in the double horseshoe image described therein. In particular, F_δ restricted to this invariant set is conjugate to the shift map on three symbols.*

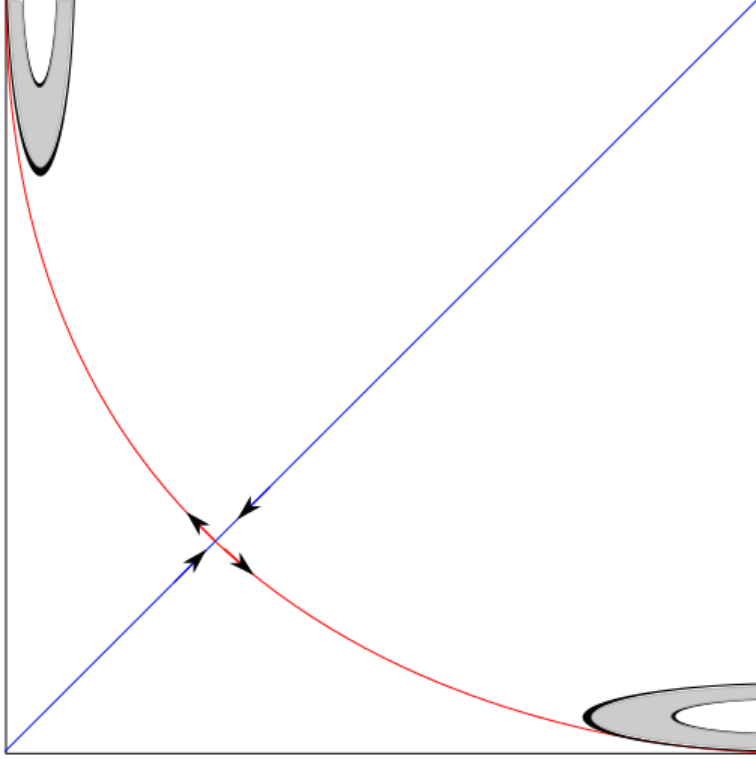


Figure 3: Embedded double horseshoe

5.2 Snap-back repeller chaos

There also are arbitrarily small C^0 perturbations of F exhibiting snap-back repeller chaos of the type described, for example, by Marotto [22, 23]. We start by showing how a small C^0 perturbation of F can turn p_* into a source with at least four snap-back points and then show that it is possible to create infinitely many snap-back points circling the fixed point. Once again we employ the s, t -coordinate system and δ_0 used in the preceding subsection to define the perturbation in a neighborhood of p_* . In particular, we define $R_\delta : \{(s, t) : |s|, |t| \leq 6\delta\} \rightarrow \mathbb{R}^2$ as

$$R_\delta(s, t) := (\phi_\delta(s), \psi_\delta(t)), \quad (17)$$

where ϕ_δ is an odd function of s defined for $s \geq 0$ as

$$\phi_\delta(s) := -2s,$$

and ψ_δ is an odd function of t defined for $t \geq 0$ by

$$\psi_\delta(t) := \begin{cases} -2t, & 0 \leq t \leq \delta \\ 2(t - 2\delta), & \delta \leq t \leq 3\delta \\ 5\delta - t, & 3\delta \leq t \leq 6\delta \end{cases},$$

and graphed in Fig. 4.

As p_* is a fixed point of both R_δ and the minimal model F , for and given $\epsilon > 0$ we can choose $0 < \delta = \delta(\epsilon) \leq \delta_0$ such that in terms of the euclidean norm, we have

$$\|F(p) - R_\delta(p)\| < \epsilon$$

for all $p \in \bar{B}_{6\sqrt{2}\delta_0}(p_*)$. As above, we are going to assume with no loss of generality, that our perturbations are actually smooth, and this leads to our next result, which is an analog of Theorem 6.

Theorem 8. *For every $\epsilon > 0$ there exists a $0 < \delta = \delta(\epsilon) \leq 0.04$ such that the (smooth) perturbation of the minimal model map F defined as*

$$F_\delta(p) := (1 - \sigma(r)) R_\delta(p) + \sigma(r)F(p), \quad (18)$$

where R_δ is as in (17), $r := \|p - p_*\|$ and

$$\sigma(r) := \begin{cases} 0, & 0 \leq r \leq 5\delta\sqrt{2} \\ (1/\delta\sqrt{2})(r - 5\delta\sqrt{2}), & 5\delta\sqrt{2} \leq r \leq 6\delta\sqrt{2} \\ 1, & r \geq 6\delta\sqrt{2} \end{cases},$$

satisfies $\|F_\delta(p) - F(p)\| < \epsilon$ for all $p \in I^2$ and p_* is a snap-back repeller for F_δ having the chaotic dynamics described in [22].

Proof. The restriction $0 < \delta \leq 0.04$ insures that $\bar{B}_{6\sqrt{2}\delta}(p_*)$ is contained in the interior of I^2 and that by taking δ sufficiently small, we can further insure that $\|F(p) - R_\delta(p)\| < \epsilon$ on $\bar{B}_{6\sqrt{2}\delta}(p_*)$. Consequently, (18) and the definition of the function σ implies that $\|F_\delta(p) - F(p)\| < \epsilon$ on I^2 . It also follows from (18) that $F_\delta(p) = R_\delta(p)$ for all $p \in \bar{B}_{5\sqrt{2}\delta_0}(p_*)$, so p_* is a hyperbolic repeller for F_δ having - as is clear from Fig. 4 - four snap-back points at $(s, t) = (0, \pm 2\delta)$ and $(s, t) = (0, \pm 5\delta)$. The chaotic dynamics then follows from [22] and the proof is complete. \square

It should be noted that the chaos described in Theorem 8 is essentially one-dimensional inasmuch as it is confined to the unstable manifold of p_* with respect to the minimal model F . However, it is not difficult to see how the construction in the above proof can be modified to obtain higher dimensional snap-back repeller chaos. One need only consider a perturbation \tilde{R}_δ given in polar form (with p_* as the origin in the s, t - coordinate plane) as

$$\tilde{R}_\delta := \psi_\delta(r) (\cos \theta, \sin \theta),$$

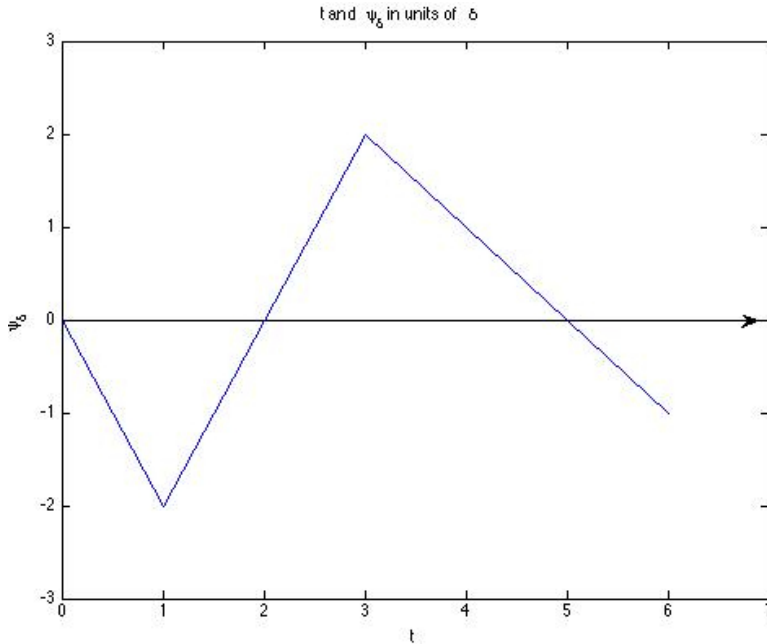


Figure 4: Coordinate function for snap-back repeller perturbation

which has two full circles of snap-back points around p_* . If in addition, we modify ψ_δ in the annulus $2\delta \leq r \leq 6\delta$ so that it is negative for certain θ -sectors, the location of the snap-back points near p_* can be easily controlled.

5.3 Chaos generated by embedding transverse homoclinic orbits and heteroclinic 2-cycles

Chaos can also be generated by perturbing F so that it has transverse homoclinic points or transverse heteroclinic 2-cycle points, for then it exhibits chaotic subshift dynamics (*cf.* [1, 10, 12, 18, 28, 33]).

To begin, we prove a simple result showing how to create transverse intersections in a homoclinic or heteroclinic curve on a surface with an arbitrarily small C^0 perturbation. It should be noted that it is well known that such transverse intersections can be produced by arbitrarily small C^1 perturbations on general C^1 surfaces (*cf.* [18, 28, 33]), but we shall find it useful for our simulations in the sequel to present a specialized C^0 result for the plane that is much easier to prove. In fact, the idea of the proof is quite transparent, involving just a carefully localized small sinusoidal perturbation normal to the homoclinic or heteroclinic curve (see Fig.5), but the details are a bit involved. By a *homoclinic curve* or *heteroclinic*

curve joining a single, respectively, pair of distinct saddle points of a differentiable map of a differentiable surface, we mean an (open) curve contained in the stable (unstable) and (stable) manifolds of the single, respectively, pair of points that contains the saddle points in its closure. A *heteroclinic 2-cycle* is just pair of heteroclinic curves joining a pair of distinct saddle points.

Lemma 9. *Let $f : S \rightarrow S$ be a C^1 self-map of connected surface S in \mathbb{R}^2 . Suppose that p and q are identical or distinct saddle points of f joined, respectively, by a homoclinic or heteroclinic curve γ that is contained both in $W^u(p) \cap W^s(q)$ and a subset of S that is compact in \mathbb{R}^2 . If there is a point $u_{-1} \in \gamma$ such that $u_0 := f(u_{-1})$, $u_1 := f^2(u_{-1})$, $u_2 := f^3(u_{-1})$ and $u_3 := f^4(u_{-1})$ are contained in a connected open neighborhood U of the closed subarc κ of γ from u_{-1} to u_3 and f is invertible on U , then there is an arbitrarily small C^0 perturbation g of f , equal to f except in an open subset V of U that contains a nontrivial closed subarc σ of κ from u_0 to a point $v_0 \in \gamma$ not containing u_1 , such that $W_g^u(p)$ has a transverse intersection with $W_g^s(q)$ in $f(\sigma)$.*

Proof. First, we orient the curve γ from p to q so that it follows the direction of positive iterates. Next, define the (oriented) arclength along γ starting from u_0 to be s , so that $s(u_0) = 0 < s(u_1) < s(u_2)$ owing to the definition of γ and the hypotheses. It follows from our assumptions that there exists a point $\tilde{u} \in \kappa$ with $0 < s(\tilde{u}) < s(u_1)$ such that the closed subarc χ of γ from u_0 to \tilde{u} satisfies the following property:

(P1) $f^{-1}(\chi)$, χ , $f(\chi)$ and $f^2(\chi)$ are pairwise disjoint closed subarcs of κ .

At each point $u \in \gamma$ there is a unit normal vector that is unique if we specify an orientation, which we do by defining the positive direction to be consistent with the right hand rule and the positive direction along the curve. We denote this vector by $\mathbf{n}(u)$, which now allows the definition of a positive and negative distance from γ points x sufficiently close to γ , which we denote by $\nu(x)$. We then combine this with a coordinate $s(x)$ defined to be $s(\phi(x))$, where $\phi(x) := u$ is the unique (for points sufficiently near γ) point on the curve such that the distance $d(x, \gamma)$ from the point x to γ is equal to $\|x - u\|$, where $\|\cdot\|$ is the Euclidean norm. Then basic results on normal bundles such as in [19] imply that there exists $\lambda_0 > 0$ such that for every $0 < \lambda \leq \lambda_0$,

$$N_\lambda := \{x \in S : s(u_{-1}) - \lambda/2 < s(x) < s(u_3) + \lambda/2; |\nu(x)| < \lambda\} \quad (19)$$

is an open set contained in U and is a neighborhood of the closed subarc κ , N_λ does not contain p or q , and it is well defined in the sense that every $x \in N_\lambda$ is uniquely determined by its coordinates $(s(x), \nu(x))$. We now have all the tools necessary to provide a simple description of small C^0 perturbations that possess the desired transverse intersections of

unstable and stable manifolds. In virtue of the differentiability of the map and the homoclinic or heteroclinic curve and the definition of N_λ , there exists $0 < \lambda_1 < \lambda_0$ such that if $0 < \lambda \leq \lambda_1$ and we define $\bar{N}_\lambda(\chi) := \{x \in S : 0 \leq s(x) \leq s(\tilde{u}); |\nu(x)| \leq \lambda\}$, then the following obtains:

(P2) $f^{-1}(\bar{N}_\lambda(\chi))$, $\bar{N}_\lambda(\chi)$, $f(\bar{N}_\lambda(\chi))$ and $f^2(\bar{N}_\lambda(\chi))$ are pairwise disjoint closed subsets of N_{λ_0} .

Now for any $0 < \epsilon < \lambda_1$, we define the perturbation increment function $\Delta_\epsilon : S \rightarrow S$ as

$$\Delta_\epsilon(x) := \begin{cases} \epsilon(1 - \lambda^{-1} |\nu(x)|) \sin\left(\frac{2\pi s(x)}{s(\tilde{u})}\right) \mathbf{n}(\phi(x)), & x \in \bar{N}_\lambda(\chi) \\ 0, & x \notin \bar{N}_\lambda(\chi) \end{cases}, \quad (20)$$

which is tantamount to saying that the s -coordinate function of Δ_ϵ is zero and ν -coordinate function is zero except in $\bar{N}_\lambda(\sigma)$ where it is defined to be the coefficient of the unit normal vector in (20). Note that this function also vanishes when $s(x) = 0$, $(1/2)s(\tilde{u})$ or $s(\tilde{u})$; that is, all along the normals to the curve γ at u_0 , \tilde{u} and a point $w \in \gamma$ with $s(\tilde{u}) < s(w) = (1/2)s(\tilde{u}) < s(\tilde{u})$. Moreover, the graph of (20) in the s, ν -plane has a transverse intersection with the s -axis at $s = (1/2)s(\tilde{u})$. The desired perturbation of f is

$$g_\epsilon = f + \Delta_\epsilon, \quad (21)$$

which is readily seen to have the desired properties. In particular, $\|g_\epsilon(x) - f(x)\| \leq \epsilon$ for all $x \in S$, $W_{g_\epsilon}^u(p) = W_f^u(p)$ and $W_{g_\epsilon}^s(q) = W_f^s(q)$ in a neighborhood of p and q , respectively, and the differentiability of both f and g_ϵ in a neighborhood of w together with (P1), (P2) and the transversality property of Δ_ϵ at w guarantee that there is a transverse intersection of $W_{g_\epsilon}^u(p)$ and $W_{g_\epsilon}^s(q)$ at $f(w)$. Thus, the proof is complete. \square

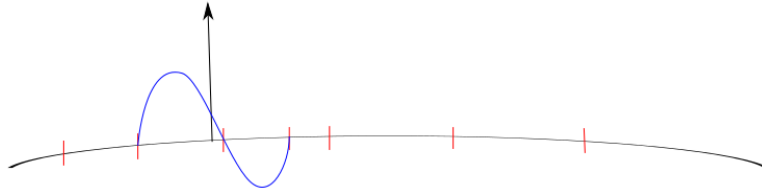


Figure 5: Transverse intersection perturbation

As a final remark concerning the above lemma, it is rather easy to see how by smoothing corners and reducing the scale of the perturbation increment, if necessary, the perturbation

of the function can be chosen to be C^1 small. Moreover, it is a simple matter to extend the result to general C^1 surfaces using standard techniques from differential geometry and topology (*cf.* [18, 19, 30, 28, 29, 33]).

Next we shall show how to embed C^0 -small dynamics in a neighborhood of the fixed point p_* of the minimal model F that has a homoclinic orbit or a heteroclinic 2-cycle. Once done, we can apply Lemma 9 to create chaotic dynamics in arbitrarily small C^0 perturbations of F . We shall use the time-one maps of the following Hamiltonian differential equations defined for $\delta > 0$ as

$$\begin{aligned}\dot{\xi} &= \eta (\delta^2 + \xi^2 + \eta^2), \\ \dot{\eta} &= \xi (\delta^2 - \xi^2 - \eta^2),\end{aligned}\tag{22}$$

which has the Hamiltonian function

$$H_\delta = (1/4) \left[(\xi^2 + \eta^2)^2 - 2(\xi^2 - \eta^2) \right].\tag{23}$$

Here we have relabeled the s, t -coordinates used in subsections 5.1 and 5.2 as ξ, η -coordinates to avoid confusion with the time parameter t in (22). This equation yields a pair of homoclinic orbits corresponding to $H_\delta = 0$ that are depicted in Fig. 6. For the heteroclinic 2-cycle, we choose the system

$$\begin{aligned}\dot{\xi} &= \eta, \\ \dot{\eta} &= -\xi + (\xi^3/\delta^2),\end{aligned}\tag{24}$$

with Hamiltonian function

$$K_\delta = (1/4) \left[2(\xi^2 + \eta^2) - (\xi^4/\delta^2) \right].\tag{25}$$

This system has a heteroclinic 2-cycle contained in $K_\delta = \delta^2/4$, which is also shown in Fig. 6. Now let the solution of (22) and (24) be denoted, respectively as

$$(\xi, \eta) = \varphi_\delta(t, (\xi_0, \eta_0))\tag{26}$$

and

$$(\xi, \eta) = \psi_\delta(t, (\xi_0, \eta_0)).\tag{27}$$

The desired embeddings are obtained from the time-1 maps of the above; namely, we define

$$\Phi_\delta(\xi, \eta) := \varphi_\delta(1, (\xi, \eta))\tag{28}$$

and

$$\Psi_\delta(\xi, \eta) := \psi_\delta(1, (\xi, \eta)).\tag{29}$$

Clearly, these maps have the desired homoclinic and heteroclinic orbits, respectively. Now, we select $\delta_0 > 0$ so small that $\bar{B}_{6\delta_0}(p_*)$ is contained in the interior of I^2 and then $0 < \delta = \delta(\epsilon) \leq \delta_0$ for a given $\epsilon > 0$ such that

$$\|F(z) - \Phi_\delta(z)\| < \epsilon \quad (30)$$

and

$$\|F(z) - \Psi_\delta(z)\| < \epsilon \quad (31)$$

for all $z \in \bar{B}_{6\delta_0}(p_*)$. Whence, we can define

$$\hat{F}_\delta(z) := (1 - \varkappa(r)) \Phi_\delta(z) + \varkappa(r)F(z) \quad (32)$$

and

$$\tilde{F}_\delta(z) := (1 - \varkappa(r)) \Psi_\delta(z) + \varkappa(r)F(z), \quad (33)$$

where $r := \|z - p_*\|$ and

$$\varkappa(r) := \begin{cases} 0, & 0 \leq r \leq 3\delta \\ (1/\delta)(r - 3\delta), & 3\delta \leq r \leq 4\delta \\ 1, & r \geq 4\delta \end{cases} . \quad (34)$$

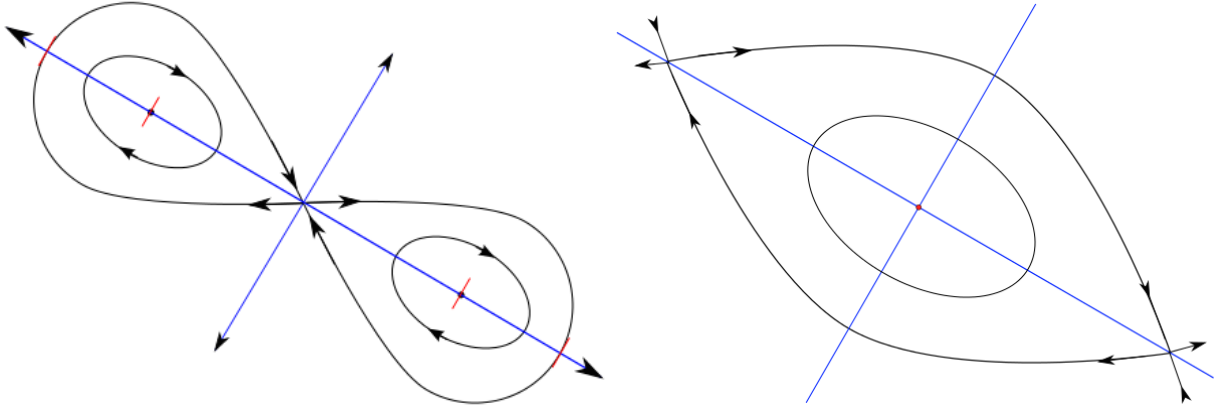


Figure 6: Embedding homoclinic and heteroclinic orbits

It follows from (24)-(33) that $\|F(z) - \hat{F}_\delta(z)\| < \epsilon$ and $\|F(z) - \tilde{F}_\delta(z)\| < \epsilon$ for all $z \in I^2$ and that \hat{F}_δ has a homoclinic orbit comprised of the stable and unstable manifolds at p_* and \tilde{F}_δ has a heteroclinic 2-cycle centered at p_* as shown in Fig. 6. Whence, we may, after choosing δ smaller if necessary, use Lemma 9 to further perturb \hat{F}_δ and \tilde{F}_δ to create a transverse intersection point in the homoclinic orbit and, respectively, to create a transverse intersection point in one or both components of the heteroclinic 2-cycle, while still remaining

ϵ -close to the original maps in the C^0 metric. Then λ -Lemma based arguments of the type developed in such sources as [1, 10, 28, 33] and the smoothing discussed above lead directly to the following result.

Theorem 10. *For every $\epsilon > 0$ there exist smooth C^0 ϵ -close perturbations of the minimal model map F exhibiting transverse homoclinic point or transverse heteroclinic 2-cycle induced chaos.*

5.4 Multihorseshoe strange attractor perturbations

The next element of our description and analysis of more pervasive chaotic C^0 perturbations of the map F defined by (3)-(4) involves embedding a symmetric pair of attracting horseshoes along the lines introduced in [15]. In particular, we shall show how to C^0 perturb F to produce multihorseshoe (more precisely, double-horseshoe) chaos (*cf.*[15], as shown in Fig. 7.

To begin the construction of the embedding, we note first that the minimal map F is actually defined and smooth at all points in the x, y -plane above the curve defined by $x + y - xy = 0$. Next, for convenience, we denote the period-2 points $(1, 0)$ and $(0, 1)$ by p and q , respectively. Let $\epsilon > 0$ be given. As both p and q are fixed points of F^2 and of G^2 , where G is the reflection in the line $y = x$, we may choose $0 < \delta \leq 1/4$ such that

$$\|F(z) - G(z)\| < \epsilon/2 \quad (35)$$

whenever $z \in \bar{B}_{10\sqrt{2}\delta}(p) \cup \bar{B}_{10\sqrt{2}\delta}(q)$. Define

$$\tilde{F}_\epsilon(z) := \begin{cases} F(z), & z \notin \bar{B}_{10\sqrt{2}\delta}(p) \cup \bar{B}_{10\sqrt{2}\delta}(q) \\ (1 - \omega(r_p))G(z) + \omega(r_p)F(z), & z \in \bar{B}_{10\sqrt{2}\delta}(p) \\ (1 - \omega(r_q))G(z) + \omega(r_q)F(z), & z \in \bar{B}_{10\sqrt{2}\delta}(q) \end{cases}, \quad (36)$$

where $r_p := \|z - p\|$, $r_q := \|z - q\|$ and

$$\omega(r) := \begin{cases} 0, & 0 \leq r \leq 8\delta\sqrt{2} \\ (1/\delta\sqrt{2})(r - 8\delta\sqrt{2}), & 8\delta\sqrt{2} \leq r \leq 9\delta\sqrt{2} \\ 1, & r \geq 9\delta\sqrt{2} \end{cases}. \quad (37)$$

It is clear from the definition and (35) that

$$\|F(z) - \tilde{F}_\epsilon(z)\| < \epsilon/2. \quad (38)$$

It now remains to make a final adjustment of the map \tilde{F}_ϵ that has the attracting horse-shoes. To this end, we define the following perturbation of the identity in $\bar{B}_{10\sqrt{2}\delta}(p) \cap I^2$ using the original x, y -coordinates

$$\Theta(x, y) = (\varphi(x), \psi(x, y)),$$

where

$$\varphi(x) := \begin{cases} 1, & x \leq 1 - 7\delta \text{ or } 1 - \delta \leq x \leq 1 \\ 2(x + \delta) - 1, & 1 - 4\delta \leq x \leq 1 - \delta \\ -2(x + 7\delta) + 3, & 1 - 7\delta \leq x \leq 1 - 4\delta \end{cases} \quad (39)$$

and

$$\psi(x, y) := \begin{cases} y/5, & x \leq 1 - 9\delta \text{ or } 1 - 5\delta \leq x \leq 1 \\ (y/5) + 6(1 - 5\delta - x), & 1 - 6\delta \leq x \leq 1 - 5\delta \\ (y/5) + 6\delta, & 1 - 7\delta \leq x \leq 1 - 6\delta \\ (y/5) + 3(x + 9\delta - 1), & 1 - 9\delta \leq x \leq 1 - 7\delta \end{cases}. \quad (40)$$

Observe that Θ has a sink at p and a saddle point at $(1 - 2\delta, 0)$ with a horizontal unstable and vertical stable manifold. Moreover, Θ maps the rectangle $[1 - 4\delta, 1 - \delta] \times [-\delta, 9\delta]$ onto a piecewise smooth (and of course smoothable) attracting horseshoe as defined in [15]. This function can be reflected in the line $y = x$ to obtain the symmetric map $\hat{\Theta} := G \circ \Theta \circ G$ mapping the rectangle $[-\delta, 9\delta] \times [1 - 4\delta, 1 - \delta]$ onto the reflection of the horseshoe image of Θ in $y = x$.

Now it follows directly from the above definitions that, taking δ smaller if necessary, we can insure that

$$\|G(z) - \Theta \circ G(z)\| < \epsilon/2 \quad (41)$$

when $z \in \bar{B}_{10\sqrt{2}\delta}(q) \cap I^2$ and

$$\|G(z) - \hat{\Theta} \circ G(z)\| < \epsilon/2 \quad (42)$$

for all $z \in \bar{B}_{10\sqrt{2}\delta}(p) \cap I^2$. Therefore, also taking into account (38), the modification F_ϵ of \tilde{F}_ϵ defined as

$$F_\epsilon(z) := \begin{cases} F(z), & z \notin \bar{B}_{10\sqrt{2}\delta}(p) \cup \bar{B}_{10\sqrt{2}\delta}(q) \\ (1 - \omega(r_p)) \hat{\Theta} \circ G(z) + \omega(r_p)F(z), & z \in \bar{B}_{10\sqrt{2}\delta}(p) \\ (1 - \omega(r_q)) \Theta \circ G(z) + \omega(r_q)F(z), & z \in \bar{B}_{10\sqrt{2}\delta}(q) \end{cases}$$

satisfies

$$\|F(z) - F_\epsilon(z)\| < \epsilon.$$

Moreover, we note that both p and q are attracting fixed points (sinks) of F_ϵ^2 , just as they are of F^2 , while $(1 - 2\delta, 0)$ and $(0, 1 - 2\delta)$ comprise a 2-cycle of F_ϵ (consisting of saddle points of F_ϵ^2) but not F . Finally, as constructed, each of the symmetric horseshoes shown in Fig. E is an attracting horseshoe of F , so that it follows from the main multihorseshoe theorem in [15] that we have now proved the following result.

Theorem 11. *For every positive ϵ there is a smooth C^0 ϵ -close perturbation F_ϵ of the minimal map F having a strange chaotic double-horseshoe attractor with attracting horseshoes in neighborhoods of the points $(1, 0)$ and $(0, 1)$.*

It is interesting to note that the strange attractor for the small perturbation of F in Theorem 11 resembles a discrete analog of the “double scroll” attractor for Chua’s circuit (cf. [6, 7]), also seen in the dynamics of RSFF realization simulations such as in [4] and could, with some minor modification, produce discrete analogs of the attractors found in the various physical circuit (ODE) models such as in [16, 17, 21, 26, 27].

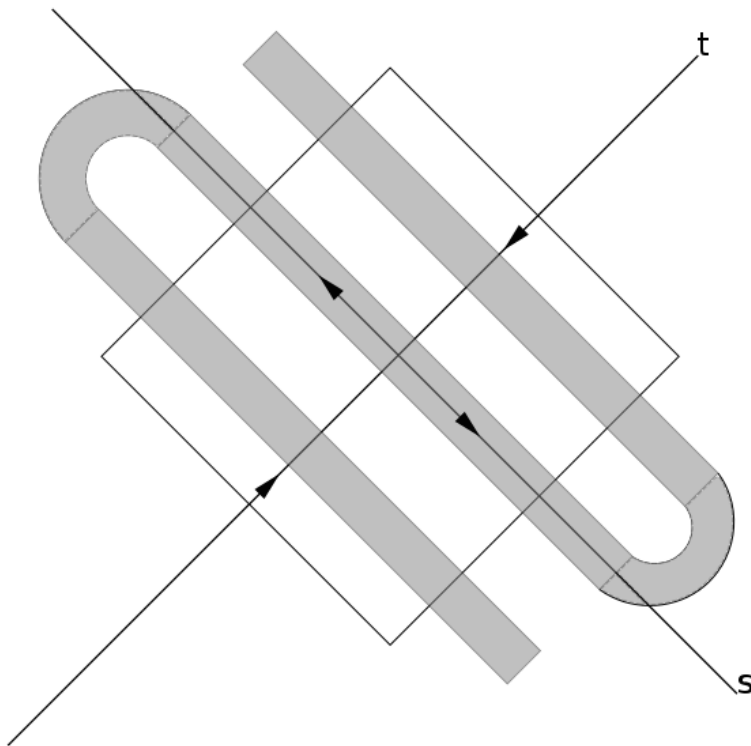


Figure 7: Embedded double-horseshoe chaotic strange attractor

5.5 Neimark–Sacker bifurcation perturbations

Our final result shall show that Neimark–Sacker bifurcations can occur in arbitrarily small C^0 perturbations of the minimal model map F . Once again, we use the ξ, η -coordinates

employed in preceding subsections to define for $\delta > 0$ the following parameter-dependent map in polar coordinates in the ξ, η - plane with origin at p_*

$$N_\delta(\xi, \eta; \mu, \alpha) := -\delta \tanh(\mu r / \delta) (\cos(\theta + \alpha), \sin(\theta + \alpha)), \quad (43)$$

where $1/2 < \mu < 3/2$, α is nonnegative and $r := \|(\xi, \eta) - p_*\|$. It is easy to verify that the origin is a global attractor of (43) for $1/2 < \mu < 1$ and a local repeller for $1 < \mu < 3/2$, so $\mu = 1$ is a bifurcation value. Moreover, as μ increases across 1 with a corresponding transition of the origin from a sink to a source, a stable invariant circle of radius $r = r(\mu)$, where $r(\mu)$ is the unique positive solution of

$$\delta \tanh(\mu r / \delta) = r. \quad (44)$$

The parameter α just represents the rotation of the map (43), so what we have is a Neimark–Sacker bifurcation at $\mu = 1$.

Now just as in the preceding subsections, we can choose $\delta_0 > 0$ so small that $\bar{B}_{6\delta_0}(p_*)$ is contained in the interior of I^2 and then $0 < \delta = \delta(\epsilon) \leq \delta_0$ for a given $\epsilon > 0$ such that

$$\|F(z) - N_\delta(z)\| < \epsilon \quad (45)$$

for all $\mu \in (1/2, 3/2)$ and $\alpha \geq 0$ whenever $z \in \bar{B}_{6\delta_0}(p_*)$. Therefore, by defining

$$\check{F}_\delta(z) := (1 - \varkappa(r)) N_\delta(z) + \varkappa(r) F(z),$$

where \varkappa is defined just as in (34), we obtain a map that is ϵ -close to F in the C^0 norm and has the desired bifurcation properties. In short, we have now proved the following result.

Theorem 12. *For every positive ϵ there is a smooth C^0 ϵ - close perturbation \check{F} of the minimal map F having a Niemark–Sacker bifurcation at p_* .*

A direct detailed construction was used for the proof of Theorem 12, but the same result can be proved, using the main theorem in [5], for any perturbation in which p_* changes from an attractor to a local repeller as a parameter is varied. It should also be noted that one can, by a straightforward modification of the above procedure, construct arbitrarily small C^0 perturbations of F exhibiting doubling Neimark–Sacker (Hopf) cascades like those in the ad hoc RSFF model analyzed in [2].

6 Simulations, Computations and Comparisons

Our purpose in this section is to show with just a few examples that our discrete dynamical model - when properly perturbed - shares many properties with actual physical realizations

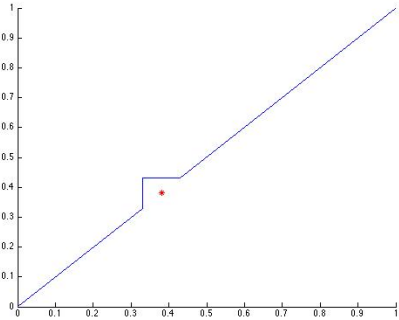
(and their associated mathematical models) of the R - S flip-flop and related circuits such as in [8, 16, 17, 21, 24, 26, 27, 31, 34]. For example, we have already demonstrated in Section 4 that our model can be perturbed so that it exhibits the chaos found by simulation in a one-dimensional map associated with the dynamics of the realization of the flip-flop circuit - which is not an R-S flip-flop circuit - investigated in [27], and it is this kind of chaos we consider in the next subsection.

6.1 Perturbed minimal model with one-dimensional chaos

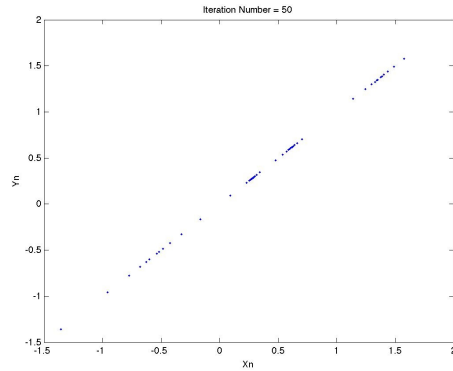
We derive the perturbed map by plugging in (13) to (4) where $x \rightarrow \phi_\sigma(x)$ and $y \rightarrow \phi_\delta(y)$,

$$\begin{aligned}\xi(x, y) &:= \frac{\phi_\delta(y)(1 - \phi_\sigma(x))}{1 - (1 - \phi_\sigma(x))(1 - \phi_\delta(y))} \\ \eta(x, y) &:= \frac{\phi_\sigma(x)(1 - \phi_\delta(y))}{1 - (1 - \phi_\sigma(x))(1 - \phi_\delta(y))}.\end{aligned}\tag{46}$$

The iterates of the perturbed map are shown in Fig. 8b.



(a) Illustration of Eq. 13.



(b) Plot of the iterates of the perturbed map.

Corollary 13. *The perturbation in the preceding theorem can be chosen so that it is a C^∞ function having the same qualitative dynamics as the function constructed above.*

6.2 Evidence of two-dimensional chaos

As we have shown above, almost any type of chaotic dynamics - including double scroll chaos - can be obtained from the ideal map by inserting specific localized perturbations. We

shall now show that the introduction of a fairly general type of small C^0 perturbation is apt to produce chaotic dynamics. In order to produce two-dimensional chaos lets use the perturbation,

$$\begin{aligned}\varphi_{k,\sigma}(x) &= 3.7[a_0 - .02 - \sum_{j=1}^k a_j \cos j\pi x] \\ a_{0,\sigma}(x) &= \frac{\mu_x + \lambda_x}{8} + \frac{\frac{1}{2} + \epsilon}{4} \\ a_{j,\sigma}(x) &= \frac{1}{2j\pi} \left\{ (1 - \lambda_x) \sin j \left(\frac{1}{2} - \epsilon \right) \pi + \frac{\mu_x + \lambda_x}{j\pi} [(-1)^j - 1] \right\}\end{aligned}$$

to get the map,

$$\begin{aligned}\xi &:= \frac{\varphi_{m,\delta}(y)(1 - \varphi_{n,\epsilon}(x))}{1 - (1 - \varphi_{m,\delta}(y))(1 - \varphi_{n,\epsilon}(x))} \\ \eta &:= \frac{\varphi_{n,\epsilon}(x)(1 - \varphi_{m,\delta}(y))}{1 - (1 - \varphi_{m,\delta}(y))(1 - \varphi_{n,\epsilon}(x))}\end{aligned}\tag{47}$$

The iterates of this map, with their characteristic splattering indicative of chaos, are shown in Fig. 8.

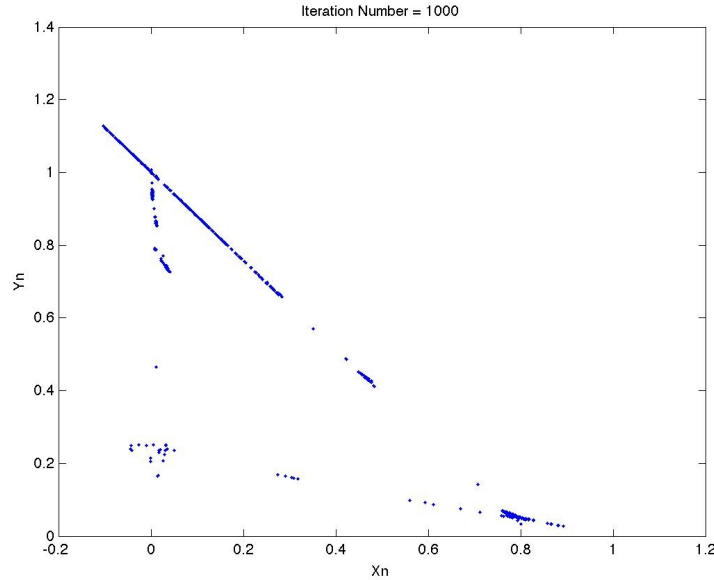


Figure 8: Iterates of a perturbed map seeming to exhibit two-dimensional chaos.

6.3 Ring oscillator example

Another interesting circuit, which we intend to analyze in detail in a forthcoming paper, is a modified ring oscillator. This ring oscillator comprises three NOR gates with feedbacks, in a very similar fashion to that of the RS flip-flop circuit. One may even choose to think of this as a three-dimensional RS flip-flop circuit.

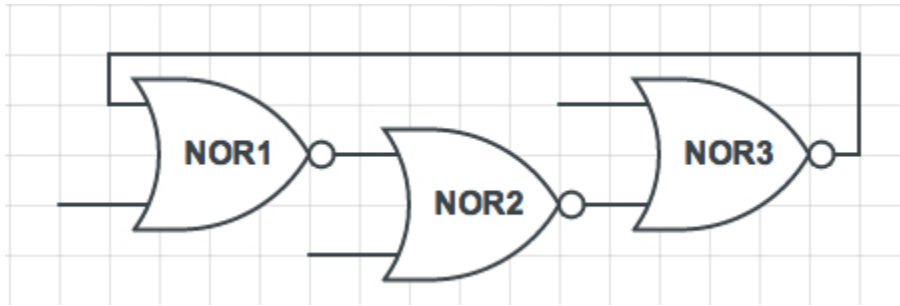


Figure 9: A schematic of a ring oscillator designed out of three NOR gates.

We note that if the inputs are set to zero, the system is precisely a ring oscillator because the NOR gates now act as inverters. Applying our algorithm for finding a discrete dynamical system model for logical circuits yields the following “ideal” (unperturbed) model,

$$\begin{aligned}
 \xi &= \frac{(x-1)(y(z-1)+1)}{(x-1)(y-1)(z-1)-1}, \\
 \eta &= \frac{(y-1)(z(x-1)+1)}{(x-1)(y-1)(z-1)-1}, \\
 \zeta &= \frac{(z-1)(x(y-1)+1)}{(x-1)(y-1)(z-1)-1};
 \end{aligned} \tag{48}$$

The only valid fixed point is $(x_*, y_*, z_*) = ((3 - \sqrt{5})/2, (3 - \sqrt{5})/2, (3 - \sqrt{5})/2)$. Since the fixed points are roots of a quartic equation, one may wonder what happens to the other roots. We find that the other three roots are out of our domain, which means that they are of no practical consequence. For the ideal model, regardless of the initial conditions, the orbits decay to the fixed point in a spiral manner shown in Fig. 10.

In order to produce more interesting dynamics we perturb the ideal model slightly. Using a perturbation similar to (47), we produce the chaotic dynamics shown in Fig. 11.

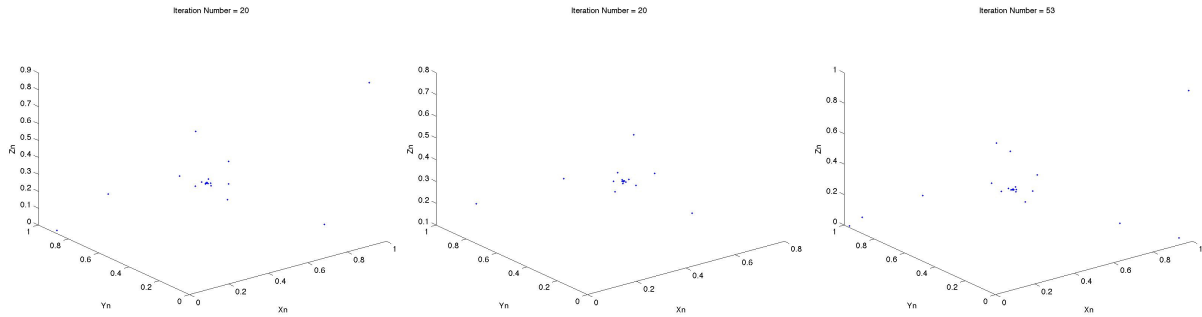


Figure 10: Plots of the orbits of Eq. 48 with initial conditions, $(.99, .1, .9)$, $(.1, .9, .2)$, and $(.1, .1, .9)$ respectively.

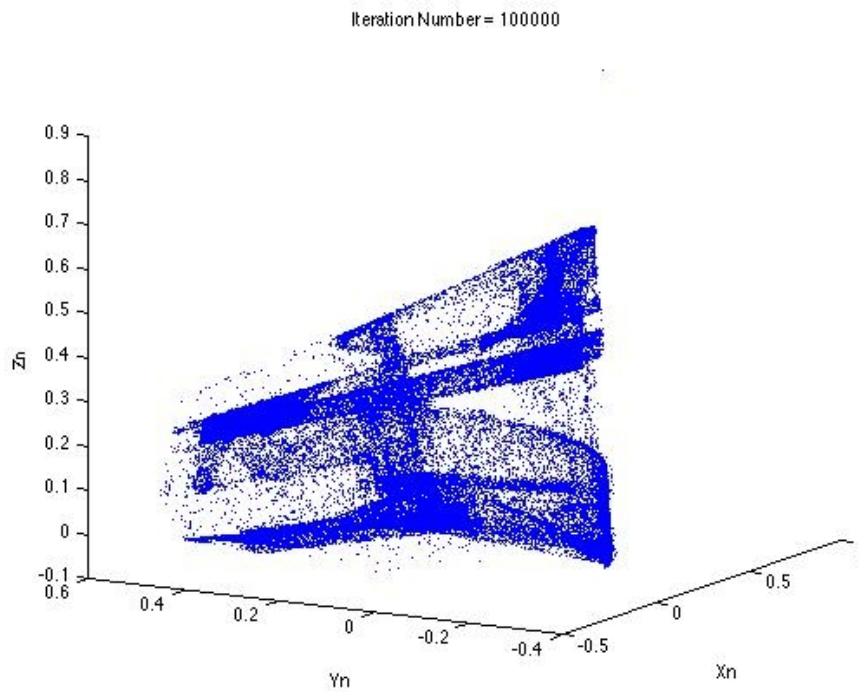


Figure 11: Plots of the orbits of the perturbed model with initial conditions $(.99, .1, .9)$.

7 Concluding Remarks

We have introduced and analyzed a rather simple discrete (ideal) dynamical model - grounded on first principles - for the RSFF circuit, which is based upon the iterates of a planar map. Moreover, we have proved that this model can be modified - by arbitrarily small C^0 perturbations - to produce just about any dynamical property observed in physical realizations of RSFF and related flip-flop circuits. We have also shown that rather general small perturbations are apt to change the structurally stable ideal model to a two-dimensional discrete dynamical system with chaotic dynamics and related artifacts such as strange chaotic attractors.

Naturally, we are planning to extend this discrete dynamical systems approach to a much wider class of logical circuits and their perturbations, and verify the effectiveness of this approach by comparing our dynamic predictions with those of more standard ODE approaches as well as experimental data extracted from actual physical circuit measurements. We also plan to address a number of related questions such as showing that logical circuit realizations represent perturbations of our ideal models in some sense, and that the perturbations can actually be characterized and quantified. Such an investigation should provide insight into the relationship that we believe exists between our discrete dynamical systems approach and the underlying discrete dynamics of reconfigurable chaotic logic gates [11].

Acknowledgements

The authors would like to thank Ian Jordan for sharing his expertise on logical circuits, which proved to be very helpful in this investigation.

References

- [1] A. Bertozzi, Heteroclinic orbits and chaotic dynamics in planar fluid flows, *SIAM J. Math. Anal.* **19** (1988), 1271-1294.
- [2] D. Blackmore, A. Rahman and J. Shah, Discrete modeling and analysis of the R-S Flip-Flop circuit, *Chaos, Solitons, and Fractals* **42** (2009), 951-963.
- [3] G. Bostock, *Programmable Logic Devices: Technology and Applications*, McGraw-Hill, New York, 1988.

- [4] D. Cafagna and G. Grassi, Chaos-based SR flip-flop via Chua's circuit, *Int. J. Bifurcation and Chaos* **16** (2006), 1521-1526.
- [5] J. Champanerkar and D. Blackmore, Pitchfork bifurcations of invariant manifolds, *Topology and Its Applications* **154** (2007), 1650-1663.
- [6] L. Chua, Chua's circuit: Ten years later, *IEICE Trans. Fundamentals* **E77-A** (1994), 1811-1821.
- [7] L. Chua, C.-W. Wu, A. Huang and G.-Q. Zhong, A universal circuit for studying and generating chaos - Part II: Strange attractors, *IEEE Trans. Circuits & Systems* **40** (1993), 745-761.
- [8] M-F. Danca, Numerical approximation of a class of switch dynamical systems, *Chaos, Solitons & Fractals* **38** (2008), 184-191.
- [9] W. de Melo, Structural stability of diffeomorphisms on two-manifolds, *Invent. Math.* **21** (1973), 233-246.
- [10] B. Deng, The Shilnikov problem, exponential expansion, strong λ -lemma, C^1 -linearization and homoclinic bifurcations, *J. Diff. Eqs.* **79** (1989), 189-231.
- [11] W. Ditto, A. Miliotis, K. Murali, S. Sinha and M. Spano, Chaogates: Morphing logic gates that exploit dynamical patterns, *CHAOS* **20** (2010), 037107.
- [12] J. Guckenheimer and P. Holmes, *Nonlinear Oscillations, Dynamical Systems, and Bifurcations of Vector Fields*, Springer-Verlag, New York, 1983.
- [13] D. Hamill, J. Deane and D. Jeffries, Modeling of chaotic DC/DC converters by iterated nonlinear maps, *IEEE Trans. Power Electron.* **7** (1992), 25-36.
- [14] P. Hartman, *Ordinary Differential Equations, 2nd ed.*, Birkhäuser, New York, 1982.
- [15] Y. Joshi and D. Blackmore, Strange attractors for asymptotically zero maps, *Chaos, Solitons & Fractals* **68** (2014), 123-138.
- [16] T. Kacprzak and A. Albicki, Analysis of metastable operation in *RS* CMOS flip-flop, *IEEE J. Solid-State Circuits* **SC-22** (1987), 57-64.
- [17] T. Kacprzak, Analysis of oscillatory metastable operation of *RS* flip-flop, *IEEE J. Solid-State Circuits* **23** (1988), 260-266.
- [18] A. Katok and B. Hasselblatt, *Introduction to the Modern Theory of Dynamical Systems*, Cambridge University Press, Cambridge, 1995.
- [19] A. Kosinski, *Differential Manifolds*, Dover, Mineola, NY, 2007.

- [20] Y. Kuznetsov, *Elements of Applied Bifurcation Theory*, 3rd ed., Springer-Verlag, New York, 2004.
- [21] G. Lacroix, P. Marchegay and N. Al Hossri, Prediction of flip-flop behavior in metastable state, *Electron. Lett.* **16** (1980), 725-726.
- [22] F. Marotto, Snap-back repellers imply chaos, *J. Math. Anal. Appl.* **63** (1978), 199-223.
- [23] F. Marotto, On redefining a snap-back repeller, *Chaos Solitons Fractals.* **25** (2005), 25-28.
- [24] J. Moser, Bistable systems of differential equations with applications to tunnel diode circuits, *IBM J. Res. Dev.* **5** (1961), 226-240.
- [25] J. Moser, *Stable and Random Motion in Dynamical Systems*, Princeton University Press, Princeton, NJ, 1973.
- [26] K. Murali, S. Sinha and W. Ditto, Implementation of a nor gate by a chaotic Chua's circuit, *Int. J. Bifurcation and Chaos* **13** (2003), 2669-2672.
- [27] H. Okazaki, H. Nakano and T. Kawase, Chaotic and bifurcation behavior in an autonomous flip-flop circuit used by piecewise linear tunnel diodes, *Proc. IEEE Int. Symp. Circuits Syst.* (ISCAS'98) Vol. III(1998), pp. 291-297.
- [28] J. Palis and W. de Melo, *Geometric Theory of Dynamical Systems*, Springer-Verlag, Berlin, 1982.
- [29] P. Percell, Structural stability on manifolds with boundaries, *Topology* **12** (1973), 123-144.
- [30] C. Robinson, Structural stability of C^1 diffeomorphisms, *J. Diff. Eqs.* **22** (1976), 28-73.
- [31] M. Ruzbehani, L. Zhou and M. Wang, Bifurcation features of a dc-dc converter under current-mode control, *Chaos, Solitons & Fractals* **28** (2006), 205-212.
- [32] S. Smale, *The Mathematics of Time*, Springer-Verlag, New York, 1980.
- [33] S. Wiggins, *Introduction to Applied Nonlinear Dynamical Systems and Chaos*, 2nd ed., Springer-Verlag, New York, 2003.
- [34] A. Zorin, E. Tolkacheva, M. Khabipov, F.-I. Buchholz and J. Niemeyer, Dynamics of Josephson junctions and single-flux-quantum networks with superconductor-normal-metal junction shunts, *Phys. Rev. B* **74** (2006), 014508.